Oxygen Reduction

DOI: 10.1002/anie.201403133

Covalent Grafting of Carbon Nanotubes with a Biomimetic Heme Model Compound To Enhance Oxygen Reduction Reactions**

*Ping-Jie Wei, Guo-Qiang Yu, Yoshinori Naruta, and Jin-Gang Liu**

Abstract: *The oxygen reduction reaction (ORR) is one of the most important reactions in both life processes and energy conversion systems. The replacement of noble-metal Pt-based ORR electrocatalysts by nonprecious-metal catalysts is crucial for the large-scale commercialization of automotive fuel cells. Inspired by the mechanisms of dioxygen activation by metalloenzymes, herein we report a structurally well-defined, bio-inspired ORR catalyst that consists of a biomimetic model compound—an axial imidazole-coordinated porphyrin—covalently attached to multiwalled carbon nanotubes. Without pyrolysis, this bio-inspired electrocatalyst demonstrates superior ORR activity and stability compared to those of the state-of-the-art Pt/C catalyst in both acidic and alkaline solutions, thus making it a promising alternative as an ORR electrocatalyst for application in fuel-cell technology.*

The activation/reduction of dioxygen is an important process in various biochemical transformations and in energy conversion systems such as fuel cells and metal–air batteries.[1,2] The oxygen reduction reaction (ORR) is a challenging reaction to catalyze, and its sluggish kinetics at the cathode is one of the key roadblocks in hydrogen–oxygen (air) fuel cells.[2a] Currently, the noble-metal platinum (Pt) is predominantly used as the ORR catalyst in fuel cells. The replacement of the scarce and costly Pt by nonprecious-metal catalysts (NPMCs) is crucial for the large-scale commercialization of automotive fuel cells. Despite significant efforts and advances in research on NPMCs in recent years, the activity and stability of those NPMCs are still lower than those of Pt-based catalysts.[3] Among various types of NPMCs explored,[3–6] metal/N/C (metal = Co, Fe) catalysts have attracted the most attention because of their low cost and facile preparation approach. The pyrolysis of cobalt- and iron-containing heteroatom precursors (e.g. metal-N_4 chelate) has been the dominant route for the preparation of NPMCs. High-temperature pyrolysis has the beneficial effects of improving both the ORR activity and durability of NPMCs; however, this method has the disadvantage in that the ORR activity cannot be tuned in a controllable structure–function manner, because the original chemical structures are completely destroyed during pyrolysis.[3d–e,4,6b] Consequently, the optimization of ORR activity mainly relies on trial-and-error-based experiments through varying the synthesis conditions, while the actual nature of the active sites and the related reaction mechanisms remain elusive with those NPMCs.

On the other hand, metalloenzymes provide us with good examples of the delicate tuning of O_2 activation/reduction processes. For example, enzymatic oxygen reduction catalyzed by cytochrome *c* oxidase (C*c*O)[7] and laccase[8] occurs at very low overpotentials. Several bioinspired NPMCs for the ORR have been reported in recent years, including a copper/heme binuclear C*c*O model,[9] multicopper complexes,[10] and iron phthalocyanines.[11] Although those unpyrolized NPMCs have demonstrated appreciable ORR activity, their ORR performance, in particular stability, is still lower than that of the Pt/C-based catalyst in acidic fuel-cell conditions. The nature of the active site of the ORR catalyst and precise control of the interfacial structure between the ORR catalyst layer and the underlying support hold the key for the development of efficient NPMCs.[12,13] Previous biomimetic mechanistic studies on the activation of O_2 with respect to the active site of C*c*O and heme-containing enzymes have shown that the incorporation of an imidazole ligand axial to iron porphyrin is crucial for O_2 activation.[14,15] With these considerations in mind, we report herein a biomimetic ORR electrocatalyst which is covalently grafted onto multiwalled carbon nanotubes (MWCNTs) and where an axial imidazole-coordinated iron porphyrin ((DFTPP)Fe-Im; DFTPP = 2,6-difluorotetraphenylporphyrin; Im = imidazole) mimics the active site of O_2-activating heme-containing enzymes (Figure 1). Noticeably, this bio-inspired (DFTPP)Fe-Im-CNTs catalyst showed superior ORR activity and stability compared to the commercial Pt/C catalyst in both acidic and alkaline environments.

The surface functionalization of MWCNTs with imidazole groups was conducted in two steps. A protected aryl alkyne monolayer was first grafted onto the MWCNTs by treating a triisopropylsilyl (TIPS) protected ethynyl aryldiazonium salt with purified MWCNTs in the presence of a hydrazine reductant. The in situ cleavage of the TIPS group afforded a grafted reactive ethynyl aryl layer on the MWCNTs, and the imidazole group was then covalently attached to the aryl alkyne monolayer through a typical "click" reaction through the use of 1-(4-azidophenyl)imidazole. We employed chemical reduction rather than electroreduction to reduce the silyl-protected aryldiazonium salt for the covalent grafting of

[*] Dr. P.-J. Wei, G.-Q. Yu, Prof.Dr. J.-G. Liu
Key Laboratory for Advanced Materials of MOE & Department of Chemistry, East China University of Science and Technology
Shanghai, 200237 (P.R. China)
E-mail: liujingang@ecust.edu.cn
Prof.Dr. Y. Naruta
Institute of Science & Technology, Chubu University
Kasugai, Aichi 487-8501 (Japan)

[**] This study was financially supported by the NSF of China (no 21271072), the Program for Professor of Special Appointment (Eastern Scholar) at Shanghai Institutions of Higher Learning, and sponsored by Shanghai Pujiang Program (no. 13J1401900).

Supporting information for this article is available on the WWW under http://dx.doi.org/10.1002/anie.201403133.

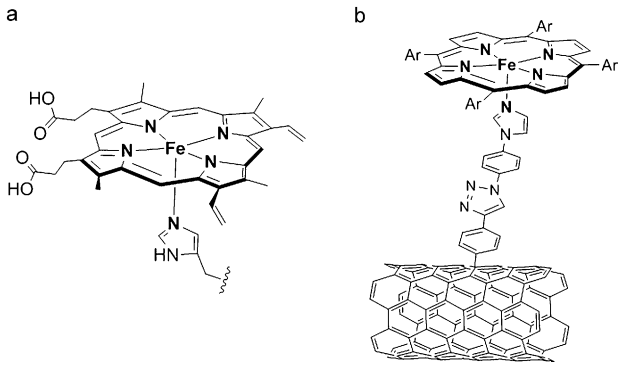

Figure 1. a) Heme (iron porphyrin) in O_2-activating enzyme active sites such as C*c*O and hemeoxygenase. b) Schematic representation of the bio-inspired ORR catalyst (DFTPP)Fe-Im-CNTs covalently anchored to the surface of multiwalled CNTs. Ar: 2,6-difluorophenyl; Im: imidazole.

MWCNTs, following a strategy similar to that of Hapiot and co-workers, who developed an efficient electrochemical approach to covalently modify carbon surfaces with controlled morphology by using a silyl-protected aryl diazonium salt.[16] The merit of this method is that it avoids the formation of disordered polyaryl multilayers on the carbon surface, thereby producing a high density of reactive groups in a monolayer-anchoring coating. The imidazole-grafted CNTs (Im-CNTs) were characterized by various spectroscopic methods. Transmission electron microscopy (TEM) and scanning electron microscopy (SEM) images showed individual CNTs (see Figure S1 in the Supporting Information). The elemental composition of the Im-CNTs was analyzed by X-ray photoelectron spectroscopy (XPS). The survey spectrum of the Im-CNTs revealed the successful incorporation of nitrogen atoms onto the CNTs with a nitrogen content of 7.88 at% (Figure 2a). The XP N_{1s} scan spectrum showed a broad peak, which was deconvoluted into two peaks with binding

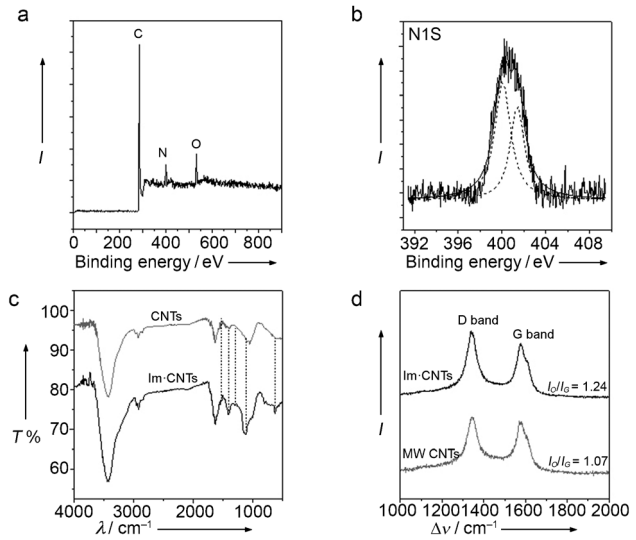

Figure 2. a) XPS survey spectrum of Im-CNTs. b) XPS N_{1s} scan spectrum of Im-CNTs. c) FTIR spectra of pristine CNTs (gray) and Im-CNTs (black). d) Raman spectra of pristine CNTs (gray) and Im-CNTs (black). Excitation = 532 nm.

energies (BEs) of 400.1 and 401.5 eV (Figure 2b). The N1s peak at 400.1 eV was assignable to the imino nitrogen atoms of the imidazole group,[17] and the nitrogen atom from the triazole ring also contributed to this peak; the peak located at 401.5 eV was attributed to the remaining nitrogen atoms of the triazole ring.[18a] A quantitative analysis of the data gave an estimate of the ratio of the grafted imidazole group to the CNTs (Im/C) as approximately 1:55 (see Table S1 in the Supporting Information). This result indicates that the modification of the surface of the CNTs with imidazole functional groups is highly efficient. Compared with that of pristine CNTs, the FTIR spectrum of the Im-CNTs revealed additional signals at 1114 and 1437 cm^{-1}, which were assignable to stretching vibrations of the triazole ring,[18b] and the remaining additional peaks may be attributable to vibrations of the imidazole-phenyl ring motif (Figure 2c). The IR results thus also suggest the formation of a triazole linker with an imidazole group on the CNTs. The Raman spectrum of the Im-CNTs displayed D and G bands at 1344 and 1576 cm^{-1}, respectively. The D/G band intensity ratio for the Im-CNTs ($I_D/I_G = 1.24$) was greater than that of the pristine CNTs ($I_D/I_G = 1.07$, Figure 2d), which indicates that more defects were created on the surface of the CNTs after covalent grafting. This phenomenon is consistent with previously reported covalent-grafted CNTs.[18a,19] Consequently, the Raman spectroscopic evidence further corroborates the successful covalent functionalization of CNTs with imidazole groups.

An iron porphyrin ((DFTPP)Fe) was assembled on the imidazole-functionalized carbon nanotubes (Im-CNTs) through coordination with the imidazole group to produce the (DFTPP)Fe-Im-CNTs catalyst. The morphology of the (DFTPP)Fe-Im-CNTs catalyst was then examined by various microscopy methods, such as TEM (Figure 3a), SEM, and atomic force microscopy (AFM; see Figure S2 in the Supporting Information). The XPS survey spectrum of the (DFTPP)Fe-Im-CNTs showed signatures of carbon, nitrogen, oxygen, fluorine, and iron (Figure 3b). The iron content was determined to be 0.84 at% by XPS analysis. The Fe_{2p} core-level XP spectrum displayed peaks at 709.9 and 722.1 eV, which were assigned to the BE values of $Fe_{2p3/2}$ and $Fe_{2p1/2}$, respectively (see Figure S3 in the Supporting Information).[20a] The N_{1s} XP spectral region of the (DFTPP)Fe-Im-CNTs showed a broad nitrogen signal, which was deconvoluted into three components (Figure 3c). The N_{1s} peaks at 399.9 and 401.4 eV were attributed to the imidazole and triazole nitrogen atoms in Im-CNTs, respectively, and the third peak at 398.8 eV was associated with the four nitrogen atoms of porphyrin.[20] The diffuse reflectance UV/Vis spectrum of (DFTPP)Fe-Im-CNTs revealed that the porphyrin Soret band appeared at 409 nm, and Q-bands appeared at approximately 500 and 592 nm, which are different from those of a simple mixture of pristine CNTs and (DFTPP)Fe, in which the Soret band appears at 422 nm (Figure 3d). This result indicated that the iron porphyrin was anchored to the CNTs most probably through the coordination of its surface-functionalized imidazole group to form an axial imidazole-coordinated porphyrin.

The ORR catalytic activity and kinetics in an O_2-saturated 0.1M $HClO_4$ solution were studied by using a rotating ring-

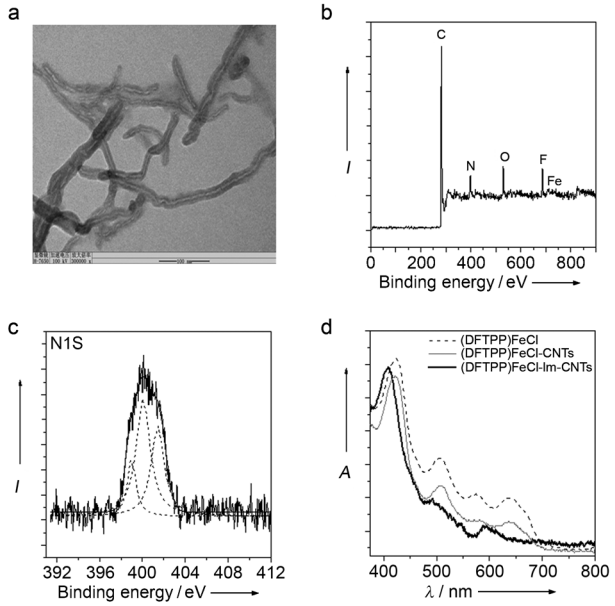

Figure 3. a) TEM image of (DFTPP)Fe-Im-CNTs. b) XPS survey spectrum of (DFTPP)Fe-Im-CNTs. c) XPS N_{1s} scan spectrum of (DFTPP)Fe-Im-CNTs. d) Diffuse reflectance UV/Vis spectra of (DFTPP)Fe-Im-CNTs (black, solid), (DFTPP)Fe-CNTs (gray, solid), and (DFTPP)Fe (gray, dashed). The Cl^- counterion is omitted for clarity.

disk electrode (RRDE) at room temperature. A commercial Pt/C catalyst (20 wt% Pt on Vulcan XC72R carbon) obtained from Johnson Matthey (JM Pt/C) was used as the reference catalyst. All electrodes were pretreated by repeated cycling of the potential between 0.0 and 1.2 V versus a reversible hydrogen electrode (RHE) at a sweep rate of 100 mV s^{-1} to remove surface contamination before testing the ORR activity. The ORR polarization curves with (DFTPP)Fe-Im-CNTs, Pt/C, and (DFTPP)Fe-CNTs (a simple mixture of pristine CNTs and the porphyrin (DFTPP)Fe catalysts are shown in Figure 4a. In a mixed kinetic/diffusion region, the half-wave potential ($E_{1/2}$) of an ORR polarization curve is often used to evaluate the electrocatalytic activity of a catalyst. The $E_{1/2}$ value for the ORR measured with the (DFTPP)Fe-Im-CNTs catalyst is 0.880 V versus RHE, which is approximately 38 mV higher than that of the Pt/C catalyst (0.842 V) under the same experimental conditions. The result demonstrated a significant improvement in the ORR kinetics by lowering the overpotential for this bio-inspired catalyst. To the best of our knowledge, the $E_{1/2}$ value of 0.880 V is the highest among the NPMCs reported to date in acid electrolytes (see Table S2 in the Supporting Information). In addition, this (DFTPP)Fe-Im-CNTs catalyst also demonstrated a significant increase in the limiting current density relative to the Pt/C catalyst at the same loading level (1.0 mg cm^{-2}). It is worth noting that the $E_{1/2}$ value for the simple mixture of (DFTPP)Fe-CNTs negatively shifted to a significantly lower potential (ca. 0.54 V) in the same acidic conditions, thus indicating its poor ORR activity (Figure 4a). The sharp contrast in the ORR activities of the (DFTPP)Fe-CNTs and (DFTPP)Fe-Im-CNTs catalysts implies the important role of the covalently grafted imidazole group, which coincides well with our previous O_2-activation mechanistic studies using similar heme-containing emzymatic models.[14]

The rotation-rate-dependent current-potential curves of the (DFTPP)Fe-Im-CNTs catalyst displayed linear Koutecky–Levich plots (Figure 4b). The electron transfer number (n) was calculated from the slopes of Koutecky–Levich plots to be about 4 at 0.55–0.70 V,[21] which suggests a nearly $4e^-$ oxygen reduction process. The amount of partially reduced product H_2O_2, as detected from the ring electrode, was less than 1% in the potential range of 0.4–0.9 V, which was even less than that of the Pt/C catalyst (Figure 4c). Kinetic currents derived from the disk currents showed a Tafel slope of about 67 mV per decade at low currents (Figure 4d). The mass-transport-corrected kinetic current at +0.90 V for the (DFTPP)Fe-Im-CNTs catalyst (2.66 mA cm^{-2}) was approximately 2.2 times higher than that of the Pt/C catalyst (1.20 mA cm^{-2}, Figure 4d inset). Accordingly, all the above results on the ORR evaluation confirm the higher ORR activity of the (DFTPP)Fe-Im-CNTs catalyst relative to the commercial JM Pt/C catalyst in acidic electrolytes.

Durability is one of the major concerns in ORR NPMCs that are used in fuel-cell technology, especially for PEMFCs. The stability of the (DFTPP)Fe-Im-CNTs catalyst was tested by chronoamperometric measurements. The (DFTPP)Fe-Im-CNTs catalyst retained about 90% of its initial current after 45000 s at 0.7 V, while the Pt/C catalyst maintained only about 57% of its initial current under the same experimental conditions (see Figure S4 in the Supporting Information). The durability of the (DFTPP)Fe-Im-CNTs catalyst was also evaluated using the US DOEs accelerated durability test protocol, where the potential was cycled between 0.6 and 1.0 V at 50 mV s^{-1} in a 0.1M $HClO_4$ solution saturated with O_2. Although a clear negative shift of $E_{1/2}$ (ca. 14 mV) was observed for the (DFTPP)Fe-Im-CNTs catalyst after 10000 continuous cycles, the negative shift of the $E_{1/2}$ value is only less than half that of the commercial Pt/C catalyst (ca. 37 mV) under the same experimental conditions (Figure 4e). After the accelerated durability test, the ORR performance gap between these two catalysts increased even further: the (DFTPP)Fe-Im-CNTs catalyst exhibited a significantly higher ORR half-wave potential ($\Delta E_{1/2:}$ ca. 60 mV) than the Pt/C catalyst (Figure 4e). These results clearly demonstrate that our bio-inspired catalyst has improved stability over the Pt/C catalyst even in acidic electrolytes. It is worth commenting that unpyrolyzed metal macrocycles and other NPMCs usually suffer from very poor durability in acidic environments.[4a,11,22] The high stability of this unpyrolyzed (DFTPP)Fe-Im-CNTs catalyst may benefit from its low overpotential for the ORR and associated high selectivity (ca. 99%) of $4e^-$ versus the $2e^-$ reduction of dioxygen to water, and, thus, less H_2O_2 is produced. The partially reduced product of H_2O_2 is notorious for its deactivation effect on the ORR catalyst, and is also the main energy loss on using O_2 as the oxidant in fuel cells. Furthermore, this catalyst effected the catalytic decomposition of H_2O_2 in argon saturated 0.1M $HClO_4$ solution with similar CV curves to those of the ORR (see Figure S10 in the Supporting Information), which suggests the catalyst has a good ability to clear H_2O_2 through

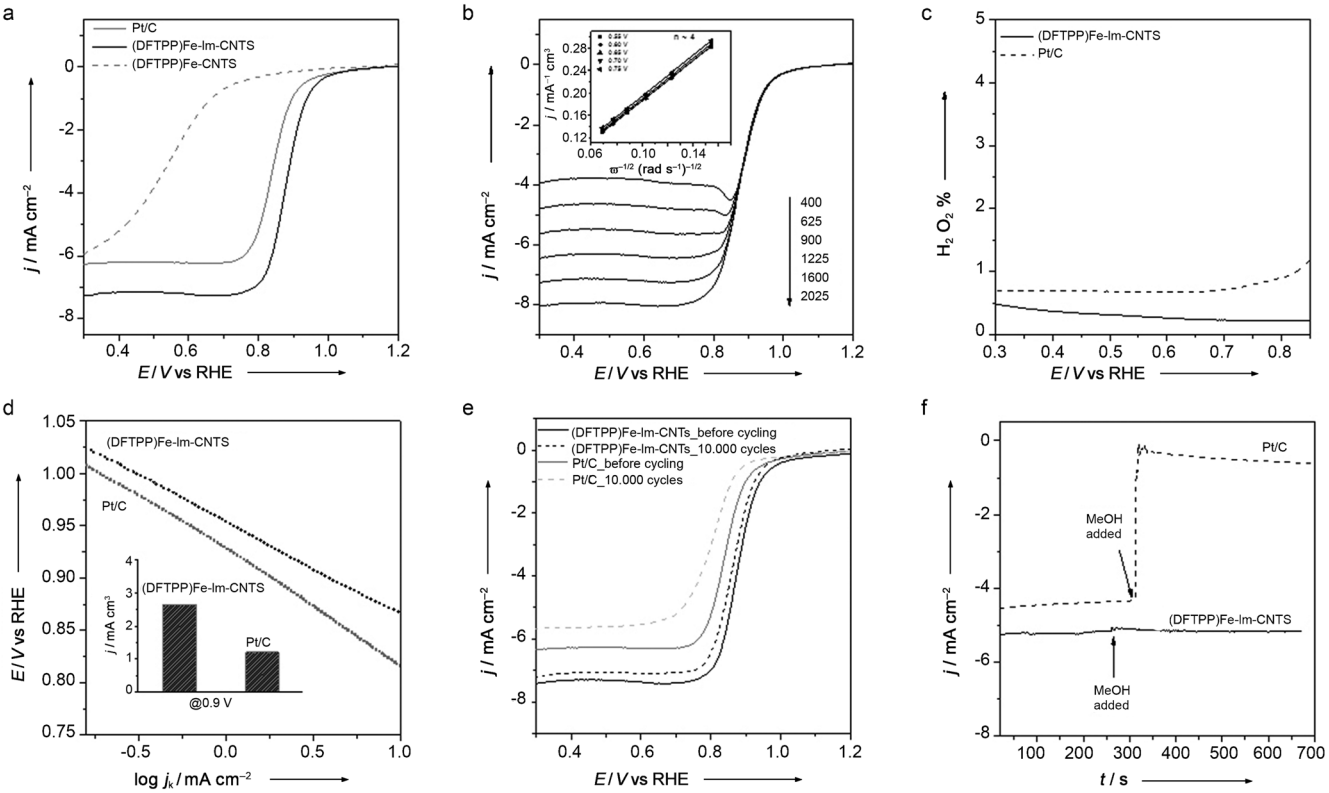

Figure 4. a) Linear scanning voltammograms of Fe(DFTPP)-CNTs (gray, dashed), (DFTPP)Fe-Im-CNTs (black, solid), and Pt/C (gray, solid) catalysts in O_2-saturated 0.1 M $HClO_4$. Electrode rotation speed, 1600 rpm; scan rate, 10 $mV s^{-1}$; loading, 1.0 $mg cm^{-2}$. b) Rotating-disk voltammograms of (DFTPP)Fe-Im-CNTs (loading 1.0 $mg cm^{-2}$) in an O_2-saturated 0.1 M $HClO_4$ solution at different rotation rates. The inset shows the corresponding Koutecky–Levich plots at different potentials. Scan rate: 10 $mV s^{-1}$. c) Peroxide yield of (DFTPP)Fe-Im-CNTs (solid) and Pt/C (dashed) catalysts in O_2-saturated 0.1 M $HClO_4$. d) Tafel plots of (DFTPP)Fe-Im-CNTs (black) and Pt/C (gray) catalysts derived by the mass-transport correction of the corresponding RDE disk currents. The inset shows the kinetic density at +0.90 V for (DFTPP)Fe-Im-CNTs and Pt/C catalysts. Electrode rotation speed, 1600 rpm; scan rate, 10 $mV s^{-1}$; e) ORR polarization plots of Pt/C (gray) and (DFTPP)Fe-Im-CNT (black) before (solid) and after (dashed) 10000 potential cycles in O_2-saturated 0.1 M $HClO_4$ solution. The potential was cycled between 0.6 and 1.0 V at a rate of 50 $mV s^{-1}$. Electrode rotation speed, 1600 rpm. f) Current–time chronoamperometric response of (DFTPP)Fe-Im-CNTs (solid) and Pt/C (dashed) upon the addition of 2.0 M methanol in an O_2-saturated 0.1 M $HClO_4$ solution. The arrow indicates the introduction of methanol. Electrode rotation speed, 900 rpm.

decomposition and reduction of the in situ produced O_2. Consequently, the catalytic activity of the (DFTPP)Fe-Im-CNTs catalyst against H_2O_2 may further contribute to its improved ORR durability.

A methanol cross-over test on the (DFTPP)Fe-Im-CNTs catalyst was also performed. The (DFTPP)Fe-Im-CNTs catalyst exhibited a stable amperometric response after the introduction of 2.0 M methanol, which suggests a good tolerance to the methanol cross-over effect. For comparison, the corresponding *i-t* chronoamperometric response of the Pt/C catalyst showed a sharp decrease in the current upon the addition of 2.0 M methanol (Figure 4 f). These results suggest that the (DFTPP)Fe-Im-CNTs catalyst may also be used as a methanol-tolerant cathode catalyst in direct-methanol fuel cells.

We also evaluated the ORR activity of the (DFTPP)Fe-Im-CNTs catalyst in 0.1M KOH electrolyte. It exhibited an ORR $E_{1/2}$ value of 0.922 V, which was approximately 47 mV higher than that of the Pt/C catalyst (0.875 V) under the same experimental conditions (see Figure S11 in the Supporting Information). The accelerated durability test was further carried out in an O_2-saturated 0.1M KOH solution. Compared to the negative shift in the $E_{1/2}$ value of the Pt/C catalyst by 34 mV, there was no apparent negative shift of the $E_{1/2}$ value for the (DFTPP)Fe-Im-CNTs catalyst after 10000 cycles, thus indicating the high stability of this bio-inspired catalyst in an alkaline environment (see Figure S15 in the Supporting Information). The (DFTPP)Fe-Im-CNTs catalyst thus also displayed both excellent ORR activity and durability in alkaline media.

In conclusion, we successfully anchored the biomimetic ORR electrocatalyst (DFTPP)Fe-Im onto the surface of carbon nanotubes through imidazole functionalization of MWCNTs. An axial imidazole-coordinated porphyrin mimics the active site of O_2-activating heme-containing enzymes. This bio-inspired ORR catalyst demonstrated a high selectivity (99%) in the direct $4e^-$ reduction of dioxygen to water, while producing the $2e^-$ reduction product of H_2O_2 in a minimal amount. This bio-inspired catalyst did not undergo any pyrolysis treatment, and exhibited remarkably higher ORR activity, superior stability, and excellent methanol tolerance in comparison to the commercial Pt/C catalyst in

both acidic and alkaline solutions. It could thus be used as a good substitute for the noble-metal Pt catalyst in energy-conversion systems in the future.

Experimental Section

The catalyst ink was prepared as follows: Catalyst (5.0 mg, (DFTPP)Fe-Im-CNTs and (DFTPP)Fe-CNTs or 20 wt% Pt on Vulcan XC-72, JM HiSPEC 3000) was mixed in a glass vial with a 5 wt% dispersion solution of Nafion (25 μL; Aldrich) and isopropanol (225 μL). The ink was sonicated in a bath sonicator for 1 h. The catalyst ink (10 μL) was applied to the surface of a glassy carbon disk (0.196 cm^2), and the solvent was evaporated at room temperature under air to produce a uniform film with a catalyst loading of about 1.0 $mg\,cm^{-2}$. The Pt loading for the reference Pt/C catalyst was 0.2 $mg_{Pt}\,cm^{-2}$.

An RRDE (Pine Instruments) with a 5.0 mm diameter glassy carbon disk and Pt ring (geometric area 0.110 cm^{-2}) was used to evaluate the catalyst performance on a CH Instrument Model 760D potentiostat in a standard three-electrode cell. To avoid any potential contamination of the catalyst by platinum, a graphite rod was used as the counter electrode. An Ag/AgCl electrode was used as the reference electrode in 0.1 M $HClO_4$ electrolyte, while a Hg/HgO electrode was used as the reference electrode in 0.1 M KOH electrolyte. All the potentials in this study were reported with respect to the reversible hydrogen electrode (RHE). All cyclic voltammetry (CV) and RRDE tests were performed at room temperature with a scan rate of 10 $mV\,s^{-1}$. The electrolyte was bubbled with O_2 for 30 min prior to each experiment, and O_2 purging was maintained over the electrolyte during the electrochemical measurements. A 30 s potential hold at the open cell potential preceded every polarization experiment. The ring potential was set to 1.3 V versus RHE.

Received: March 8, 2014
Revised: April 15, 2014
Published online: May 19, 2014

Keywords: bioinorganic chemistry · electrochemistry · enzymes models · oxygen · reduction

[1] a) E. G. Kovaleva, J. D. Lipscomb, *Nat. Chem. Biol.* **2008**, *4*, 186 – 193; b) W. Nam, *Acc. Chem. Res.* **2007**, *40*, 522 – 531; c) C. E. Tinberg, S. J. Lippard, *Acc. Chem. Res.* **2011**, *44*, 280 – 288; d) J. Hohenberger, K. Ray, K. Meyer, *Nat. Commun.* **2012**, *3*, 720.

[2] a) M. K. Debe, *Nature* **2012**, *486*, 43 – 51; b) F. Y. Cheng, J. Chen, *Chem. Soc. Rev.* **2012**, *41*, 2172 – 2192.

[3] a) R. Bashyam, P. Zelenay, *Nature* **2006**, *443*, 63 – 66; b) M. Lefèvre, E. Proietti, F. Jaouen, J.-P. Dodelet, *Science* **2009**, *324*, 71 – 74; c) G. Wu, K. L. More, C. M. Johnston, P. Zelenay, *Science* **2011**, *332*, 443 – 447; d) G. Wu, *Acc. Chem. Res.* **2013**, *46*, 1878 – 1889; e) F. Jaouen, E. Proietti, M. Lefevre, R. Chenitz, J.-P. Dodelet, G. Wu, H. T. Chung, C. M. Johnstonb, P. Zelenay, *Energy Environ. Sci.* **2011**, *4*, 114 – 130.

[4] a) Z. Chen, D. Higgins, A. Yu, L. Zhang, J. Zhang, *Energy Environ. Sci.* **2011**, *4*, 3167 – 3192; b) R. Othman, A. L. Dicks, Z. Zhu, *Int. J. Hydrogen Energy* **2012**, *37*, 357 – 372.

[5] Y. Zheng, Y. Jiao, M. Jaroniec, Y. Jin, S. Z. Qiao, *Small* **2012**, *8*, 3550 – 3566.

[6] a) S. Guo, S. Zhang, S. Sun, *Angew. Chem. Int. Ed.* **2013**, *52*, 8526 – 8544; *Angew. Chem.* **2013**, *125*, 8686 – 8705; b) A. Morozan, B. Jousselme, S. Palacin, *Energy Environ. Sci.* **2011**, *4*, 1238 – 1254.

[7] a) D. A. Proshlyakov, M. A. Pressler, C. DeMaso, J. F. Leykam, D. L. DeWitt, G. T. Babcock, *Science* **2000**, *290*, 1588 – 1591; b) M. Wikström, *Biochim. Biophys. Acta Bioenerg.* **2012**, *1817*, 468 – 475.

[8] a) N. Mano, J. L. Fernandez, Y. Kim, W. Shin, A. J. Bard, A. Heller, *J. Am. Chem. Soc.* **2003**, *125*, 15290 – 15291; b) J. A. Cracknell, K. A. Vincent, F. A. Armstrong, *Chem. Rev.* **2008**, *108*, 2439 – 2461.

[9] J. P. Collman, N. K. Devaraj, R. A. Decréau, Y. Yang, Y.-L. Yan, W. Ebina, T. A. Eberspacher, C. E. D. Chidsey, *Science* **2007**, *315*, 1565 – 1568.

[10] M. S. Thorum, J. Yadav, A. A. Gewirth, *Angew. Chem. Int. Ed.* **2009**, *48*, 165 – 167; *Angew. Chem.* **2009**, *121*, 171 – 173.

[11] a) W. Li, A. Yu, D. C. Higgins, B. G. Llanos, Z. Chen, *J. Am. Chem. Soc.* **2010**, *132*, 17056 – 17058; b) R. Cao, R. Thapa, H. Kim, X. Xu, M. G. Kim, Q. Li, N. Park, M. Liu, J. Cho, *Nat. Commun.* **2013**, *4*, 2076.

[12] A. A. Gewirth, M. S. Thorum, *Inorg. Chem.* **2010**, *49*, 3557 – 3566.

[13] F. Sedona, M. D. Marino, D. Forrer, A. Vittadini, M. Casarin, A. Cossaro, L. Floreano, A. Verdini, M. Sambi, *Nat. Mater.* **2012**, *11*, 970 – 977.

[14] a) J.-G. Liu, Y. Naruta, F. Tani, *Angew. Chem. Int. Ed.* **2005**, *44*, 1836 – 1840; *Angew. Chem.* **2005**, *117*, 1870 – 1874; b) J.-G. Liu, T. Ohta, Y. Yamaguchi, T. Ogura, S. Sakamoto, Y. Maeda, Y. Naruta, *Angew. Chem. Int. Ed.* **2009**, *48*, 9262 – 9267; *Angew. Chem.* **2009**, *121*, 9426 – 9431; c) J.-G. Liu, Y. Shimizi, T. Ohta, Y. Naruta, *J. Am. Chem. Soc.* **2010**, *132*, 3672 – 3673; d) T. Ohta, J.-G. Liu, Y. Naruta, *Coord. Chem. Rev.* **2013**, *257*, 407 – 413.

[15] a) K. D. Karlin, *Nature* **2010**, *463*, 168 – 169; b) M. T. Kieber-Emmons, M. F. Qayyum, Y. Li, Z. Halime, K. O. Hodgson, B. Hedman, K. D. Karlin, E. I. Solomon, *Angew. Chem. Int. Ed.* **2012**, *51*, 168 – 172; *Angew. Chem.* **2012**, *124*, 172 – 176; c) S. P. de Visser, J. S. Valentine, W. Nam, *Angew. Chem. Int. Ed.* **2010**, *49*, 2099 – 2101; *Angew. Chem.* **2010**, *122*, 2143 – 2146.

[16] Y. R. Leroux, H. Fei, J.-M. Noel, C. Roux, P. Hapiot, *J. Am. Chem. Soc.* **2010**, *132*, 14039 – 14041.

[17] V. Feyer, O. Plekan, S. Ptasinska, M. Iakhnenko, N. Tsud, K. C. Prince, *J. Phys. Chem. C* **2012**, *116*, 22960 – 22966.

[18] a) T. Palacin, H. L. Khanh, B. Jousselme, P. Jegou, A. Filoramo, C. Ehli, D. M. Guldi, S. Campidelli, *J. Am. Chem. Soc.* **2009**, *131*, 15394 – 15402; b) H.-X. Wang, K.-G. Zhou, Y.-L. Xie, J. Zeng, N.-N. Chai, J. Li, H.-L. Zhang, *Chem. Commun.* **2011**, *47*, 5747 – 5749.

[19] C. Gao, Y. Z. Jin, H. Kong, R. L. D. Whitby, S. F. A. Acquah, G. Y. Chen, H. Qian, S. R. P. Silva, S. Henley, P. Fearon, H. W. Kroto, D. R. M. Walton, *J. Phys. Chem. B* **2005**, *109*, 11925 – 11932.

[20] a) L. Preda, C. Negrila, M. F. Lazarescu, M. Anastasescu, G. Dobrescu, E. Santos, V. Lazarescu, *Phys. Chem. Chem. Phys.* **2011**, *13*, 17104 – 17114; b) F. Buchner, K. Flechtner, Y. Bai, E. Zillner, I. Kellner, H.-P. Steinruck, H. Marbach, J. M. Gottfried, *J. Phys. Chem. C* **2008**, *112*, 15458 – 15465.

[21] A. J. Bard, L. R. Faulken, *Electrochemical Methods: Fandamental and Applications*, 2nd ed., Wiley-VCH, New York, **2001**.

[22] a) N. Cheng, C. Kemna, S. Goubert-Renaudin, A. Wieckowski, *Electrocatalysis* **2012**, *3*, 238 – 251; b) J. Masa, K. Ozoemena, W. Schuhmann, J. H. Zagal, *J. Porphyrins Phthalocyanines* **2012**, *16*, 761 – 784.

